Effects of Mesoscale Eddies On Intraseasonal Variability of Intermediate Water East of Taiwan

Qiang Ren
Institute of Oceanology, Chinese Academy of Sciences
Fei Yu (yuf@qdio.ac.cn)
Institute of Oceanology, Chinese Academy of Sciences
Feng Nan
Institute of Oceanology, Chinese Academy of Sciences
Yuanlong Li
Institute of Oceanology, Chinese Academy of Sciences
Jianfeng Wang
Institute of Oceanology, Chinese Academy of Sciences
Yansong Liu
Institute of Oceanology, Chinese Academy of Sciences
Zifei Chen
Institute of Oceanology, Chinese Academy of Sciences

Research Article

Keywords: Intraseasonal variation, Intermediate Water, Kuroshio, Mesoscale eddies, Eastern Taiwan

Posted Date: January 4th, 2022

DOI: https://doi.org/10.21203/rs.3.rs-1198576/v1

Abstract

The variability of intermediate water (IW) east of Taiwan was investigated utilizing 17 months of long-term, continuous and synchronous measurements of temperature, salinity and current from mooring sites deployed at 122ºE/23ºN from January 2016 to May 2017. For the first time, we prove that the intraseasonal variability in the IW within significant periods of ~80 days was caused by mesoscale eddies propagating westward from the Subtropic Counter Current (STCC) area. The correlation coefficients between sea level anomalies (SLAs) and the Kuroshio, and between SLAs and the minimum salinity in the intermediate layer, were 0.63 and 0.52, respectively. The anticyclonic (cyclonic) eddies from the STCC, increased (decreased) the speed of the Kuroshio as well as increase (decrease) the temperature and salinity in the 400–600 m in east of Taiwan. Combines Archiving, Validation and Interpretation of Satellite Oceanographic (AVISO) products data, showed that temperature and salinity increased (decreased) in the intermediate layer due to the downward (upward) vertical movement of the water mass by anticyclonic (cyclonic) eddies. Anticyclonic eddies strengthened the Kuroshio and benefitted SCSIW flowing through the Luzon Strait to enhance salinity, while cyclonic eddies weakened the Kuroshio and favored relatively low-salt NPIW, in the area east of Taiwan.

Introduction

The Kuroshio is a strong western boundary current in the North Pacific Ocean that originates from the North Equatorial Current. It brings heat and salt from low latitudes to mid and high latitudes and has an important impact on air-sea interactions and climate change along its path (Kwon et al., 2010; Qiu & Chen, 2010; Zhang et al., 2001). Therefore, understanding the characteristics of the Kuroshio water masses is of great significance for studying its poleward volume, heat and salinity transport and for making future climate predictions.

According to present classifications, the Kuroshio water masses in the Northwest Pacific evolved from the subtropical circulation of water masses in the North Pacific. The Kuroshio water masses are mainly divided into subsurface water and intermediate water. Subsurface Kuroshio water, also known as Kuroshio tropical water (KTW), evolves from North Pacific tropical water (NPTW) and is mainly located at depths of 150~250 m with maximum salinity in its subsurface layers; it is distributed throughout most of the Northwest Pacific (Rudnick et al., 2011). In addition, KTW is characterized by high temperatures and salinity (Chen, 2005; Mensah et al, 2015;Nitani, 1972).

Intermediate Kuroshio water is widely distributed in the North Pacific and cold with relatively low salinity at depths of 400~800 m; it has a minimum salinity of approximately 34.10–34.20 psu and a potential density of 26.8 σ_θ, which generally refers to North Pacific Intermediate Water (NPIW) (Gordon et al., 2014; Talley, 1993). The NPIW primarily originates in the Okhotsk Sea and is transported via the Oyashio current along Kuril Island and east of the Japanese island of Hokkaido (Mensah et al., 2014, 2015; Yasuda, 1997; You et al., 2003). Then, NPIW spreads throughout the North Pacific and can extend southward to ~15°N by the subtropical gyre; it has even been found in the Halmahera eddy (HE) (Kashino et al., 1999). At the

same time, NPIW is transported through the Luzon Strait to the South China Sea where it forms South China Sea Intermediate Water (SCSIW) with a salinity minimum of approximately 34.4 psu at core depths of approximately 500 m (Lan et al., 2012; Liu et al., 2012; You et al., 2005). In addition, many studies defined another water mass, referred to as Kuroshio Intermediate Water (KIW), along the western boundary from Luzon Island to an area east of Taiwan, according to plots of the average temperature versus salinity (θ-S) of the Kuroshio (Chen, 2005; Chern & Wang, 1998; Mensah et al., 2014; Nakamura et al., 2013). However, these papers report different sources of KIW. Mensah et al. (2014) claim that KIW is mostly found in the West Philippine Sea Basin along the Kuroshio, with saltier variations in NPIW. According to Chern and Wang (1998), Chen (2005), and Nakamura et al. (2013), KIW may contain both SCSIW and NPIW and is mostly found east of Taiwan.

During ongoing research on intermediate water east of Taiwan, many discussions concern the presence of SCSIW east of Taiwan. In previous work, SCSIW with a salinity of approximately 34.4 psu was found on the continental shelf northeast of Taiwan (Chen & Huang, 1996; Chern & Wang, 1998). In a survey of the Luzon Strait and the Okinawa Trough, Chen (2005) also found evidence of SCSIW spreading to southern Japan though water east of Taiwan. Nakamura et al. (2013) used climatological data to describe IW east of Taiwan as a mixture of SCSIW and NPIW. Recently, Mensah et al. (2015) used temperature data at 580 m to develop an empirical formula to estimate IW salinity; they found that IW east of Taiwan contains SCSIW and NPIW. Mensah et al. (2015) also showed that IW salinity correlated with thickness of the Kuroshio. However, Chern and Wang (1998) did not identify SCSIW in the water north of Green Island, according to survey data from several hydrographic sections in the water east of Taiwan, and they claimed that the ridge between Taiwan and Green Island (less than 500 m deep) blocks the northward flow of water from the northern part of the South China Sea ,and thus, prevents SCSIW from being carried into the area east of Taiwan. These findings suggest that intermediate waters along the Kuroshio east of Taiwan are highly variable, and researchers speculate that SCSIW and NPIW may alternate below the core of the Kuroshio.

Actually, most of the studies of IW in the area east of Taiwan use only a small amount of sectional data acquired during surveys and provide characteristics at a given point in time. Due to the lack of simultaneous long-term continuous observations of the temperature, salinity and currents in this area, knowledge of the properties of IW east of Taiwan is remain limited, and this knowledge is not sufficient to clearly reveal the distribution characteristics and variations of IW in this area. For the first time, it has been possible to study the variations and processes of IW east of Taiwan using 17 months of simultaneous and continuous measurements of temperature, salinity and current. A subsurface mooring was deployed at 23°N, 122°E (red triangle in Figure 1) from January 2016 to May 2017 to monitor the temperature, salinity and current upper 800 m. Figure 1b shows a schematic diagram of the water mass distribution and circulation east of Taiwan. As an area with a high incidence of mesoscale eddies propagating westward from the Subtropic Counter Current (STCC), the Kuroshio east of Taiwan is affected by mesoscale eddies and experiences intraseasonal variability with periods of 80~100 d (Andres et al., 2017; Chang el al., 2011; Chang et al., 2018; Hsin et al., 2010; Jan et al., 2015; Jan et al., 2017; Johns et al., 2001; Lee et al., 2013; Ren et al., 2020; Tsai et al., 2015; Zhang et al., 2001). Although

Mensah et al. (2015) hypothesized in his paper that the variation of IW are related to mesoscale eddies, whether IW in the intermediate layer is influenced by mesoscale eddies needs to be determined by direct measurement data, more than that the variation characteristics of IW and the relationship between IW and the Kuroshio are also not clearly.

Data

Mooring system data

The Institute of Oceanography, Chinese Academy of Sciences (IOCAS), conducted a large-scale survey of the Western Pacific in January 2016. During this survey, we deployed a subsurface mooring east of Taiwan at a water depth of 4900 m; in May 2017, we successfully recovered the mooring system using the research vessel R/V *Science* (location: 122°E, 23°N, Figure 1). Figure S1 shows a simplified schematic diagram of the configuration and deployment of the subsurface mooring buoy system. The main floating ball integrated two up-looking and down-looking 75 kHz Acoustic Doppler Current Profilers (ADCPs) manufactured by Teledyne RD Instruments (TRDI), designed for use at depths of approximately 400 m, to measure currents at depths above 800 m according to the following parameters: the measurement interval was 1 hour, the number of depth cells was 74, the bin size was 8 m, and the number of pings was 30 per measurement. At depths of 400–1000 m, we used conductivity-temperature-depth meters (CTDs, type: SBE37, manufactured by Sea Bird Instrument) at intervals of 100 m, and the sampling interval was 10 minutes. The current data from the ADCPs were controlled for quality, including a good threshold of 70% and a cutoff of 2 m/s for current speed. To filter out the influence of high-frequency signals, all current and CTD data were averaged daily for this study.

AVISO altimetry and salinity data

An Archiving, Validation, and Interpretation of Satellite Data in Oceanography (AVISO) altimetry dataset was used in this paper. The sea level anomaly (SLA) and geostrophic current data were obtained from the commercial AVISO Global ARMOR3D L4 Reprocessed dataset (http://marine.copernicus.eu/services-portfolio/access-to-products/). The SLA data had spatial resolution of 1/4° × 1/4°, and the dataset extended approximately 17 months, from January 2016 to June 2017.

To analyze the temperature and salinity changes of IW, we selected the commercial data of Global Ocean Multi Observation Products, which is based on Global Ocean Observations (GOOPs). This commercial dataset is based on global ocean observations, using sea surface temperature (SST), sea level abnormalities (SLAs), average dynamic terrain (MDT) and temperature (T) and salinity (S) in situ vertical profiles. At present, there are weekly and monthly mean 3D data for temperature, salinity, Ug, Vg and sea surface height data, and the spatial resolution is 1/4°. The vertical direction from 0 to 5500 m is divided into 33 layers (0, 10, 20, 30, 50, 75, 100, 125, 150, 200, 250, 300, 400, 500, 600, 700, 800, 900, 1000, 1100,

1200,1300, 1400, 1500, 1750, 2000, 2500, 3000, 3500, 4000, 4500, 5000, and 5500 m). The commercial data are very similar to our on-site observations, and the RMS error is lower than the climatic field.

Results

Time series of measurement current and intermedaite water

Because the main float of the mooring system was affected by the current, its depth changes greatly, which led to deviations of the entire mooring system. Therefore, all the instruments and equipment designed for use at a predetermined depth were basically in a fluctuating state. The daily average salinity in Figure 2b shows large fluctuations for a maximum floating depth of 300 m.

The results for the current show the velocity structure and variation characteristics of the Kuroshio (Figure 2a). The maximum velocity of the Kuroshio can reach 1.0 m/s, and it can influence vertical depths to 800 m based on 0.2 m/s isotach, which is clear defined as the main poleward flow velocity of the Kuroshio (Chang et al., 2018; Jan et al., 2015). Figure 2b shows the average velocity of each layer with large velocities and velocity variations in the uppermost 400 m, which indicates the main depth of the Kuroshio in the vertical direction. The velocity deviation above 200 m is approximately 0.25 m/s, which is approximately one-half the magnitude of the velocity, indicating the instability of the Kuroshio velocity east of Taiwan. Of course, this instability may be caused by a variety of factors, such as the propagation of mesoscale eddies in the western direction, the movement of the Kuroshio main axis, etc. The most significant variation in the Kuroshio east of Taiwan is expressed as intraseasonal variations with periods of ~85 d, and these variations are mainly modulated by mesoscale eddies propagating westward from the STCC (Ren et al., 2020). The relationship between significant intraseasonal variations in the Kuroshio and IW is the focus of this study. The minimum salinity (S_{min}) at the core of the intermediate water, shown in Figure 2c, is found mainly in the potential density range of 26.6–26.8 σ_θ, where S_{min} is approximately 31.5 psu and the depth is approximately 600 m. We also found that S_{min} at the core showed discontinuous variability; for example, S_{min} at the core was approximately 600 m during the period March-April 2016, and S_{min} was approximately 550 m by September 2016. There are 7 results for S_{min} at the core in the observation period, according to the total measurement time, and an intraseasonal variation period of approximately 70–80 days was estimated. The mean salinity of each layer is shown in Figure 2d, and the black line shows the deviation of the salinity. Although the overall standard deviation was relatively small, the variance was larger at 440 m than in the other layers, indicating a relatively large variation in salinity in the middle layer.

T-S characteristics of Intermediate water

To more clearly analyze the characteristics of IW east of Taiwan, we drew a T-S scatter plot of data obtained from the moored CTDs (Figure 3a). For comparison, historical data from the Argo international project for average temperature and salinity east of Taiwan but away from the Kuroshio area (box A1 in Figure 1.1a) and the South China Sea area (box A2 in Figure 1.1a) represent NPIW and SCSIW, respectively. The S_{min} values of NPIW and SCSIW are 34.18 psu and 34.39 psu, respectively.

The main characteristics of IW in the water east of Taiwan are as follows: S_{min} varies from 34.15 psu to 34.4 psu, corresponding to a temperature change in the range of 7 to 8°C and a potential density variation of 26.6–26.8 σ_θ for S_{min}, respectively. The salinity distribution near the characteristic salinity value of NPIW is denser (near the red curve in Figure 3a), indicating that the overall characteristics of the water mass are closer to those of NPIW during the observations. There were only two moments in time when S_{min} exceeded 34.39 psu, as shown in Figure 3a, indicating that observations of IW with typical SCSIW characteristics are relatively infrequent. That is, most of the time, IW in the water east of Taiwan resembles a mixture of NPIW and SCSIW. This water mass was also defined as Kuroshio Intermediate Water (KIW) by earlier studies (Chen, 2005; Chern & Wang, 1998; Nakamura et al., 2013). Mensah et al. (2015) that reported that SCSIW could not flow directly to eastern Taiwan due to blocking by the Green Islands in southeastern Taiwan, but NPIW and SCSIW could mix at the relatively southern location of the Luzon Strait, and the Kuroshio carried this water mass to the east of Taiwan.

Therefore, we can obtain the typical average characteristics of this water mass, and the average θ-S curves are plotted in Figure 3a (blue curve). S_{min} and the corresponding temperature of this water mass were 34.28 psu and 7.5°C, respectively. The core was located at 550 m, which corresponded to a depth between the S_{min} core depths of 500 m for SCSIW and 600 m for NPIW.

To explore the proportions of NPIW and SCSIW in KIW east of Taiwan, the mixing ratio of the two water masses was calculated using the concentration mixing formula according to the following method. First, salinity values of 34.19 psu and 34.39 psu were taken to characterize NPIW and SCSIW, respectively, according to the red and green curves in Figure 3a, and the S_{min} of each profile measured by the CTDs was taken to be the value of the two mixtures. Then, these three values were introduced into the concentration equation to calculate the mixing ratio. Figure 3b shows that the proportion of NPIW in KIW was relatively high, and 70% of the time, the NPIW mixing ratio exceeded 60%. There were approximately 7 moments in time when the proportion of NPIW reached 100%, which meant that there was basically only NPIW in the area east of Taiwan; these moments were evenly distributed during the observation period. The longest duration lasted for approximately one month in September 2016. Meanwhile, there were 4 moments when the proportion of NPIW was very small, such as March 2016, July 2016, August 2016, and June 2017. The proportion of NPIW in July 2016 and June 2017 was almost zero, indicating that there was basically no NPIW east of Taiwan, and SCSIW was predominant.

The above results show the great variability of IW found east of Taiwan, with some moments where SCSIW was directly observed, and other times when these was almost no evidence of SCSIW. In fact, the results of previous studies basically used the temperature and salt data of cruise sections to study

intermediate water masses, but sectional data can only provide characteristics at certain moments, which are variable and cannot represent overall behavior. Therefore, their sectional data are insufficient for analyzing whether SCSIW is present east of Taiwan. Our direct observations explain the ambiguous results about the presence of SCSIW east of Taiwan from the previous study.

Intraseasonal variability of IW

The results of the power spectrum analysis of the salinity in the 500 m layer (Figure 4b) show that IW east of Taiwan had a significant intraseasonal period of 70–80 days. Through a reverse calculation of salinity based on an empirical temperature-salinity formula, Mensah et al. (2015) reported that the intraseasonal period of IW east of Taiwan was ~100 days. Compared with the result of Mensah et al. (2015), the intraseasonal signal of IW obtained from directly measured salinity data in this study may be more realistic reflection of the variation characteristics of the water mass. Of course, it is also possible that the difference in results is due to the timing of the two observations.

To better understand the intraseasonal variability, the meridional velocity anomaly, temperature and salinity anomaly were calculated by subtracting the average value during the observation of each layer from the average daily mooring data displayed in Figure 5b-d. The meridional velocity anomalies are basically consistent and banded in the 0–800 m range, and temperature and salinity anomalies also exhibit synchronization in the 400–800 m range. The alternating band structures of positive and negative shapes are clearly shown in the anomalous temperature and salinity graphs, also indicating an intraseasonal signal of approximately 3 months. The maximum negative and positive salinity anomalies were -0.12 psu and 0.1 psu, and the maximum negative and positive temperature anomalies were -1.5°C and 2°C, respectively. During the observation period, there were 6 negative salinity anomalies in 17 months, March-April, June, September-October, and November-December in 2016 and January-February and April-May in 2017; the positive anomalies occurred during the other observation times. Meanwhile, the temperature and salinity anomalies were consistent and showed synchronous changes. The distribution of the integrated current anomalies showed that at most moments, positive meridional velocity anomalies corresponded to positive anomalies of temperature and salinity, while negative meridional velocity anomalies corresponded to negative anomalies of temperature and salinity. The relatively consistent variation in current, temperature and salinity suggests that all three parameters may be influenced by the same factor.

Dissussion

Intraseasonal variability of IW caused by mesoscale eddies

Actually, we know that the source of intraseasonal signals in the water east of Taiwan is mainly generally eddy activities, which has been proven by many studies ((Hsin et al., 2010; Jan et al., 2015; Ren et al., 2020; Tsai et al., 2015; Zhang et al., 2001). The power spectrum of the SLAs shows a period of

approximately 80 days in Figure 4a, which is almost the same as the periodic signal of IW, indicating a possible relationship between mesoscale eddies and IW. Also, we checked the local wind stress has a period of ~15 days (figure not shown) is inconsistent with the ~80 day variability of the IW. This maybe indicates that the local wind is not a direct cause of the intraseasonal variability of the IW. To identify the relationship between mesoscale eddies, Kuroshio velocity and IW, we plotted the time series of the SLAs; the salinity averages were between 26.4 and 27.0 σ_θ and the Kuroshio velocity averages between 0 and 400 m are shown in Figure 6a. The results showed that they exhibited significantly consistent variations, with correlation coefficients of 0.63 and 0.52 between the SLA and Kuroshio velocity and between the SLA and salinity, respectively. Figure 6b and 6c show scatter plots of the measured potential temperature against salinity in the range 26.4–27.0 σ_θ, composite with the SLAs and V, respectively. Most of the fresher (saltier) water corresponded to negative (positive) SLAs displayed in Figure 6b. Additionally, stronger currents carry saltier water, while only weak currents can carry lower temperature and fresher water; this is especially significant in the case of the southward-flowing current shown in Figure 6c. The above results indicate that changes in the synchronization of temperature, salinity, and current were highly correlated with SLAs. From Figure 5a, the typical westward propagation characteristics of mesoscale eddies were found along the 23°N section east of Taiwan; combined with V, salinity and temperature anomalies, they revised the corresponding relationships with SLAs. These results suggest that the positive (negative) SLAs caused by westward propagation of anticyclonic (cyclonic) eddies from the STCC increases (decreases) the speed of the Kuroshio while increasing (decreasing) temperature and salinity at approximately 400–600 m. In other words, changes in both temperature and salinity in the intermediate layer and the Kuroshio can be traced to mesoscale eddies coming from the west.

To further analyze the time-scale relationship between mesoscale eddies and IW, we constructed a lag correlation coefficient diagram of salinity in the range 26.4–27.0 σ_θ and SLAs within the region 119–130°E/18–25°N (Figure 7). Figure 7a-g show that salinity lagged behind SLAs during days 0–60 days with an interval of 10 days. East of Taiwan, there was an area with a positive correlation coefficient (red) that gradually moved westward with time from the 60th day onward, and the correlation coefficient increased, with its maximum increasing from 0.3 on the 60th day to 0.5 on the 0th day. There was a significant area with a positive correlation coefficient located at 125°E/22°N with a 60-day lag relative to the mooring site, while at the highest area located at 122°E/22.5°N with 0 lag time; as a result, the estimated westward propagation velocities of the mesoscale eddies were approximately 10 cm/s. As a comparison, Tsai et al. (2015) used PIES data to conclude that the westward speed of an eddy near Taiwan was in the range of 11–24 cm/s. Also, the westward propagation speed of mesoscale eddies of first-mode baroclinic Rossby waves near 20°N was approximately 8 cm/s (Qiu & Chen, 2010).

Possible mechanism of IW variations

Measurements at the mooring site, a single point, are not enough to reflect the movement of salinity and the current-water mass relationship. Therefore, a wider range of Global Ocean Multi Observation Products (GOOP) data from global ocean observation was used to analyze this behavior. First, we examined the

consistency between data from the moored CTDs and GOOP. The time series chart of GOOP salinity data is shown in Figure S2 and compared to salinity data from the moored system in Figure 2c. The salinity characteristics corresponded better at several moments, e.g., the low salinity characteristics in January, April, June, September, and November 2016 and January and May 2017, and the relatively high salinity characteristics in the period from July to August 2016, than at other times. Although the agreement was not complete, it is enough to indicate that the variation characteristics of salinity from AVISO are similar to those from the in situ measurements.

Actually, the salinity at the intermediate layer was analyzed according to horizontal and vertical movement. First, we constructed the vertical structure of the anticyclonic and cyclonic eddy times to discuss IW movement in the vertical direction. Figure 8a-d show the anomalous temperature and salinity distributions from 0 to 1000 m along the center of cyclonic and anticyclonic eddies, respectively. In anticyclonic (cyclonic) eddies, isothermal and isosalinity lines showed obvious concave (convex) structures corresponding to vertical downward (upward) movement of the water mass at the center. The vertical temperature anomaly was positive (negative), while the anomalous salinity structure was divided into two layers below 100 m. This process revealed that the downward movement of the upper layer of relatively high-temperature water caused positive temperature anomalies during anticyclonic eddies, while during cyclonic eddies, the upward movement of water caused negative temperature anomalies. However, the structure was different for temperature and salinity because the water mass east of Taiwan was divided into subsurface high-salinity water at 100–200 m and intermediate fresher water at 400–600 m. The downward movement of water at the centers of the anticyclonic eddies caused subsurface high-salinity water to flow downward and mix with relatively fresh water in the intermediate layer and cause positive anomalies above 600 m; as fresher intermediate water moved downward, it caused negative anomalies in the deep layer below 600 m. When the cyclonic eddies occurred, the upward movement of center water caused negative temperature anomalies inside entire cyclonic eddies. The salinity structure displayed negative anomalies above 600 m and positive anomalies below 600 m in cyclonic eddies, as shown in Figure 8d. With the upward movement of the water mass, fresher intermediate water mixed with high salinity water and caused negative salinity anomalies in upper intermediate layers. At the same time, the high salinity of the deep water moving upward caused positive salinity anomalies in the deep layer. From the above analysis of salinity movement in the vertical direction, the results show that temperature and salinity increased (decreased) in intermediate layers due to vertical movement of water by anticyclonic (cyclonic) eddies east of Taiwan.

The above analysis only considers vertical movement of water induced by mesoscale eddies. Next, we discuss horizontal movement of water combined with currents in intermediate layers. Figure 9a and b show composite circulation and salinity for cyclonic and anticyclonic eddy interactions, with the Kuroshio average in the range of 26.4–26.8 σ_θ east of Taiwan.

Figure 9a and b show different salinity distribution characteristics in the South China Sea and Northwestern Pacific, in which SCSIW is typically higher than NPIW. When cyclonic eddies impinge on the Kuroshio (Figure 9a), the current is weakened by cyclonic eddies, and relatively fresher water surrounds

the intermediate layer east of Taiwan. Additionally, Figure 9a shows that little water is carried out of the SCS by the Kuroshio, which means that NPIW more easily dominates water east of Taiwan and maintains lower salt characteristics. In contrast, during anticyclonic interactions with the Kuroshio, the current is strengthened to the north, and the field of salinity is significantly higher in the intermediate layer along Luzon Island to the Taiwan coast (Figure 9b). Meanwhile, more SCSIW is carried by currents and mixes with NPIW, increasing salinity east of Taiwan during anticyclonic eddies. As a result, the mooring area is dominated by a stronger northward current and relatively saltier water. Therefore, the results reveal that horizontal movement of IW carried by current is possible as follows. Anticyclonic eddies strengthened the Kuroshio and benefitted SCSIW flowing through the Luzon Strait, leading to an increase in salinity east of Taiwan. While cyclonic eddies weakened the Kuroshio and reduced SCSIW outflow from the Strait, this was conducive to relatively low-salt NPIW occupying the area east of Taiwan.

Summary

This study utilizes 17 months of long-term, continuous and synchronous measurements of temperature, salinity and current data from a mooring site located at 122°E/23°N east of Taiwan. The IW characteristics in eastern Taiwan were revealed as follows: S_{min} varied from 34.15 psu to 34.4 psu, corresponding to a temperature variation in the range from 7 to 8°C and a potential density variation of 26.6–26.8 σ_θ for S_{min}. We observed pronounced intraseasonal variations in IW with periods of ~80 days.

For the first time, We prove that ISVs of IW are caused by mesoscale eddies propagating westward from the STCC area. In our observations with moored instruments, the Kuroshio also had strong ISVs, and correlations between the current, IW and SLA were significant. The SLAs not only influenced the Kuroshio but also brought intraseasonal signals to the water mass of the intermediate layer. The correlation coefficients between SLAs and current and between SLAs and minimum salinity in the intermediate layer were 0.63 and 0.52, respectively.

Our results showed that positive (negative) SLAs, caused by the westward propagation of anticyclonic (cyclonic) eddies from the STCC, increased (decreased) the speed of the Kuroshio, also increase (decrease) the temperature and salinity in the 400–600 m in east of Taiwan. By using the map of correlations between SLAs and S_{min}, the westward propagation speed of the mesoscale eddies was estimated to be approximately 10 cm/s.

Combined the GOOP data, the movement of IW are discussed. The vertical movement of IW showed that the temperature and salinity increased (decreased) in the intermediate layer due to the vertical movement of water by anticyclonic (cyclonic) eddies. Meanwhile, during the horizontal movement of the water mass, anticyclonic eddies strengthened the Kuroshio and benefitted SCSIW flowing through the Luzon Strait, leading to an increase in salinity east of Taiwan. While the cyclonic eddies weakened the Kuroshio and reduced SCSIW outflow from the Strait, conditions were conducive to relatively low-salt NPIW in the area east of Taiwan.

Declarations

Acknowledgments, Samples, and Data

This research is supported by the National Key Research and Development Plan (Nos. 2017YFC1403401, 2016YFC1400505), the Global Climate Change and Air-sea Interaction Program (Nos. GASI-02-PAC-ST-Wwin, GASIIPOVAI-01-06), the National Natural Science Foundation of China (No. 41676005), and the NSFC Innovative Group Grant (No. 41421005). We would like to thank all the personnel of the R/V Science for their contribution to the data acquisition. The data provided by AVISO are also greatly appreciated. The mooring data that support this study are available from the corresponding author upon request.

References

1. Andres, M., V. Mensah, S. Jan,M.-H. Chang, Y.-J. Yang, C. M. Lee,B. Ma, and T. B. Sanford. Downstream evolution of the Kuroshio's time-varying transport and velocity structure, *Journal of Geophysical Research.Oceans*,122, 3519–3542 (2017).
2. Chang M-H, Jan S, Mensah V, Andres M, Rainville L, Yang Y J, Cheng Y-H. Zonal migration and transport variations of the Kuroshio east of Taiwan induced by eddy impingements. *Deep-Sea Research Part I-Oceanographic Research Papers*, 131: 1–15 (2018).
3. Chang Y L, Oey L Y. Interannual and seasonal variations of Kuroshio transport east of Taiwan inferred from 29 years of tide-gauge data. *Geophysical Research Letters*, 38 (2011).
4. Chen, C. T. A. Tracing tropical and intermediate waters from the South China sea to the Okinawa trough and beyond. *Journal of Geophysical Research*, *110*(C5) (2005).
5. Chen, C. T. A., & Huang, M. H. A mid-depth front separating the South China sea water and the Philippine sea water. *Journal of Oceanography*, *52*(1), 17–25 (1996).
6. Chern, C., & Wang, J. The spreading of the South China sea water to the east of Taiwan during summertime. *Acta Oceanographica Taiwanica*, *36*, 97–110 (1998).
7. Gordon, A. L., Flament, P., Villanoy, C., & Centurioni, L. The nascent Kuroshio of lamon bay. *Journal of Geophysical Research: Oceans*, *119*(7), 4251–4263 (2014).
8. Hsin, Y. C., Qu, T., & Wu, C. R. Intra-seasonal variation of the Kuroshio southeast of Taiwan and its possible forcing mechanism. *Ocean Dynamics*, *60*(5), 1293–1306 (2010).
9. Jan, S., Yang, Y. J., Wang, J., Mensah, V., Kuo, T. H., Chiou, M. D., et al. Large variability of the Kuroshio at 23.75°N east of Taiwan. *Journal of Geophysical Research: Oceans*, *120*(3), 1825–1840 (2015).
10. Jan, S., Mensah, V., Andres, M., Chang, M., & Yang, Y.. Eddy-Kuroshio Interactions: Local and Remote Effects. *Geophysical Research Letters*, 122(12), 9744–9764 (2017).
11. Kashino, Y., Watanabe, H., Herunadi, B., Aoyama, M., & Hartoyo, D.. Current variability at the pacific entrance of the indonesian throughflow. *Journal of Geophysical Research: Oceans*, 104 (1999).

12. Kwon, Y. O., Alexander, M. A., Bond, N. A., Frankignoul, C., Nakamura, H., Qiu, B., & Thompson, L. A. Role of the Gulf stream and Kuroshio–oyashio systems in large-scale atmosphere–ocean interaction: a review. *Journal of Climate*, *23*(12), 3249–3281 (2010).
13. Lan, J., Zhang, N., & Wang, C. The destiny of the North Pacific intermediate water in the South China sea. *Acta Oceanologica Sinica*, *31*(5), 41–45 (2012).
14. Lee, IH., Ko, D.S., Wang, YH. et al. The mesoscale eddies and Kuroshio transport in the western North Pacific east of Taiwan from 8-year (2003–2010) model reanalysis. *Ocean Dynamics*, 63, 1027–1040 (2013).
15. Liu, C., Wang, D., Chen, J., Du, Y., & Xie, Q. Freshening of the intermediate water of the South China sea between the 1960s and the 1980s. *Chinese Journal of Oceanology and Limnology*, *30*(6), 1010–1015 (2012).
16. Mensah, V., Jan, S., Chang, M. H., & Yang, Y. J. Intraseasonal to seasonal variability of the intermediate waters along the Kuroshio path east of Taiwan. *Journal of Geophysical Research: Oceans, 120*(8), 5473–5489 (2015). Mensah, V., Jan, S., Chiou, M. D., Kuo, T. H., & Lien, R. C. Evolution of the Kuroshio Tropical water from the luzon strait to the east of Taiwan. *Deep Sea Research Part I: Oceanographic Research Papers, 86*, 68–81 (2014).
17. Nakamura, H., Nishina, A., Liu, Z., Tanaka, F., Wimbush, M., & Park, J. H. Intermediate and deep water formation in the Okinawa Trough. *Journal of Geophysical Research: Oceans*, *118*(12), 6881–6893 (2013).
18. Nitani, H. Beginning of the kuroshio. In H. Stommel, K. Yoshida (Eds.), *Kuroshio: Its physical aspects* (pp. 129–163). Tokyo: University of Tokyo Press. (1972).
19. Qiu, B., & Chen, S. Interannual variability of the north pacific subtropical countercurrent and its associated mesoscale eddy field. *Journal of Physical Oceanography*, *40*(1), 213–225 (2010).
20. Ren, Q., Yu, F., Nan, F., Wang, J., & Xu, A. Intraseasonal variability of the Kuroshio east of Taiwan, China, observed by subsurface mooring during 2016–2017. *Journal of Oceanology and Limnology*, *38*(5), 1408–1420 (2020).
21. Rudnick, D., Jan, S., Centurioni, L., Lee, C., Lien, R. C., Wang, J., et al. Seasonal and mesoscale variability of the Kuroshio near its origin. *Oceanography*, *24*(4), 52–63 (2011).
22. Talley, L. D. Distribution and formation of North Pacific intermediate water. *Journal of Physical Oceanography*, *23*(3), 517–537 (1993).
23. Tsai, C. J., Andres, M., Jan, S., Mensah, V., Sanford, T. B., Lien, R. C., & Lee, C. M. Eddy-Kuroshio interaction processes revealed by mooring observations off Taiwan and Luzon. *Geophysical Research Letters*, *42*(19), 8098–8105 (2015).
24. Yasuda, I. The origin of the North Pacific intermediate water. *Journal of Geophysical Research: Oceans*, *102*(C1), 893–909 (1997).
25. You, Y. The pathway and circulation of North Pacific intermediate water. *Geophysical Research Letters*, *30*(24). (2003).

26. You, Y., Chern, C. S., Yang, Y., Liu, C. T., Liu, K. K., & Pai, S. C. The South China Sea, a cul-de-sac of North Pacific intermediate water. *Journal of Oceanography*, *61*(3), 509–527 (2005).
27. You, Y., Suginohara, N., Fukasawa, M., Yoritaka, H., Mizuno, K., Kashino, Y., & Hartoyo, D. Transport of North Pacific intermediate water across Japanese WOCE sections. *Journal of Geophysical Research*, *108*(C6) (2003).
28. Zhang, D., Lee, T. N., Johns, W. E., Liu, C. T., & Zantopp, R. The Kuroshio east of Taiwan: Modes of variability and relationship to interior ocean mesoscale eddies. *Journal of Physical Oceanography*, *31*(4), 1054–1074 (2001).

Figures

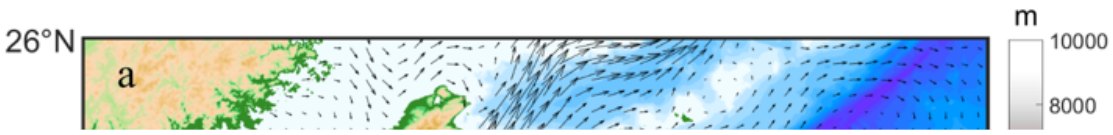

Figure 1

The surface geotrophic currents and a schematic diagram of the water mass distribution around the eastern Taiwan. (**a**) Isobaths (in meters) from data according to the ETOPO1 Global Relief Model (color shading) and average surface geotropic currents between Jan 2016 and May 2017 from AVISO data (vectors). For analysis of properties of IW in this study, the average characteristics of the water masses in two typical regions were selected to represent North Pacific Intermediate Water (in the red A1 box) and

South China Sea Intermediate Water (in the green A2 box). (**b**) Schematic diagram of the water mass distribution and circulation east of Taiwan. The mooring system was deployed from Jan 2016 to May 2017. The topographic data from following website: https://www.ngdc.noaa.gov/mgg/global/etopo1sources.html

Figure 2

Time series of meridional velocity and salinity from mooring observation. (**a**) The daily mean of the ADCP measurements of the meridional velocity (V) above 800 m and (**b**) the mean velocity with standard deviation. The black contour in (a) indicates the 0.2 m/s line of the velocity. (**c**) The daily mean of the CTD measurements of the salinity at depths from 350 m to 800 m during the period from Jan 2016 to April 2017 and (**d**) the mean salinity with standard deviation. Gray in (**c**) indicates the potential density calculated from temperature, salinity and depth data measured by the CTDs. The red lines in (**b**) and (**d**) indicate the means, and the black lines in (**b**) and (**d**) indicate the deviations, of the velocity and salinity, respectively.

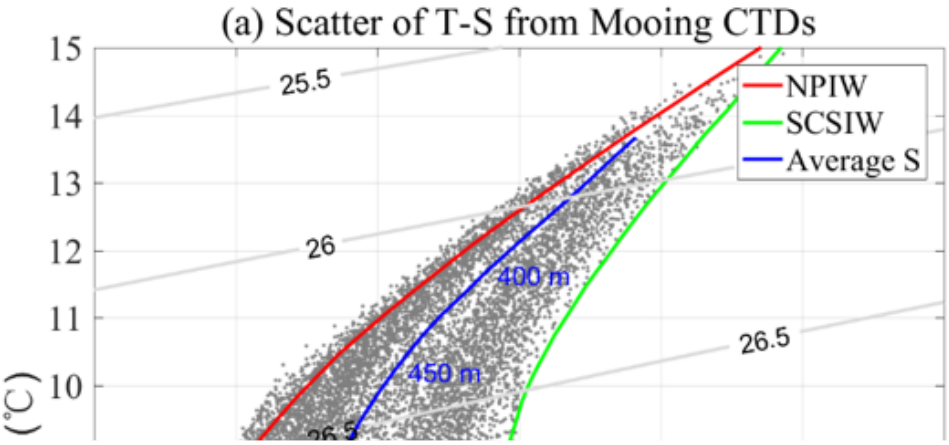

Figure 3

T-S scatter plot and time series of minimum salinity**. (a)** T-S scatter diagram obtained from moored CTD measurements. The gray points are CTD data, the red and green curves are the average temperature and salinity curves obtained from historical Argo data in the range of box A1 in Figure 1.1a, and box A2 in Figure 1.1a. **(b)** The time series of minimum salinity (orange curve) and the proportion of NPIW (green curve).

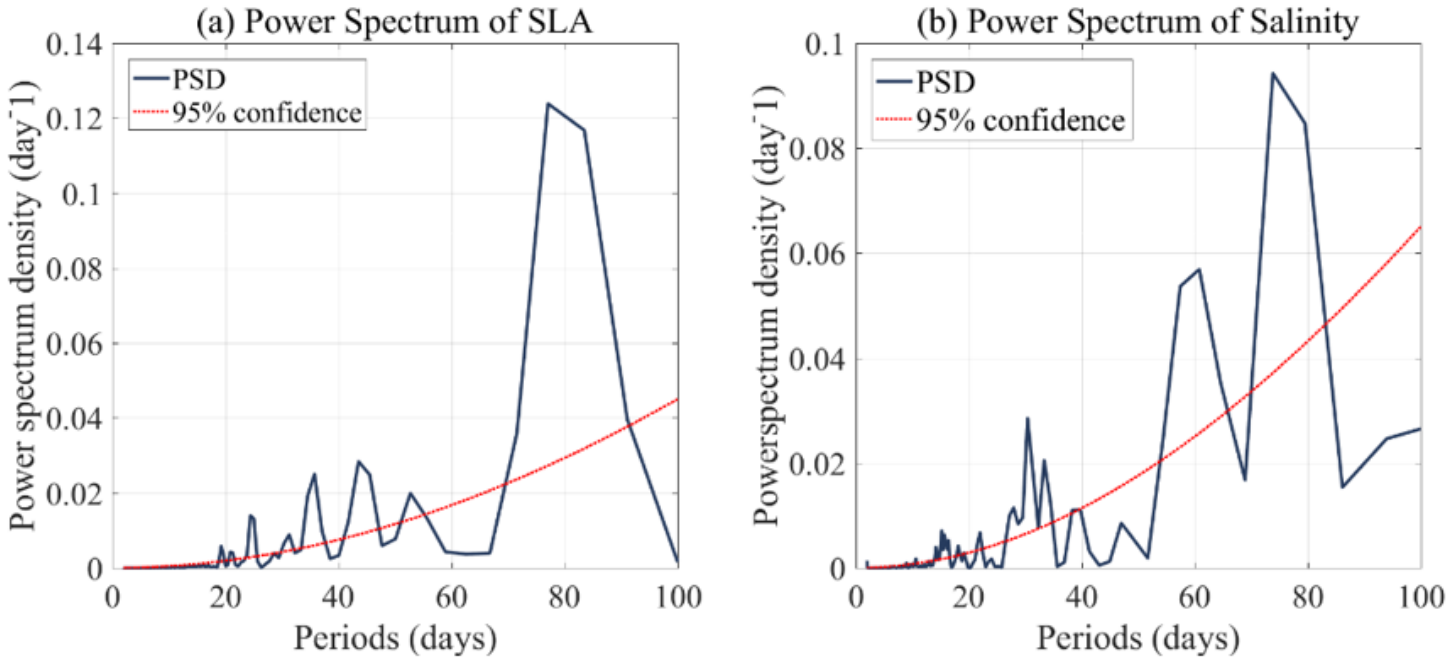

Figure 4

Power spectrum of SLA and salinity. (**a**) The PSD of the SLA at a mooring location from AVISO data and (**b**) the PSD of the salinity from moored CTD measurements, respectively. The red dashed line indicates the 95% confidence level.

Figure 5

The SLA and anomaly of meridional velocity, temperature and salinity. (**a**) The longitude-time contours of the SLAs along 23 °N; (**b**) meridional velocity anomaly from 0 to 800 m; (**c**) salinity anomaly from 400 to 800 m; (**d**) temperature anomaly from 400 to 800 m. The meridional velocity, temperature and salinity anomalies were subtracted from the average values at each level over the entire observation time. The black contours indicate the zero-line values.

Figure 6

The relationship between the SLA, current and salinity in the intermediate layer. (**a**) Plot of 20–100 day bandpass-filtered time series of SLAs (blue curve), minimum salinity (green curve) and average velocity in the 0–400 m range (red curve). The salinity and velocity data are shown in (**b**) a T-S scatter diagram where the color indicates SLAs and (**c**) a T-S scatter diagram where the color indicates velocity.

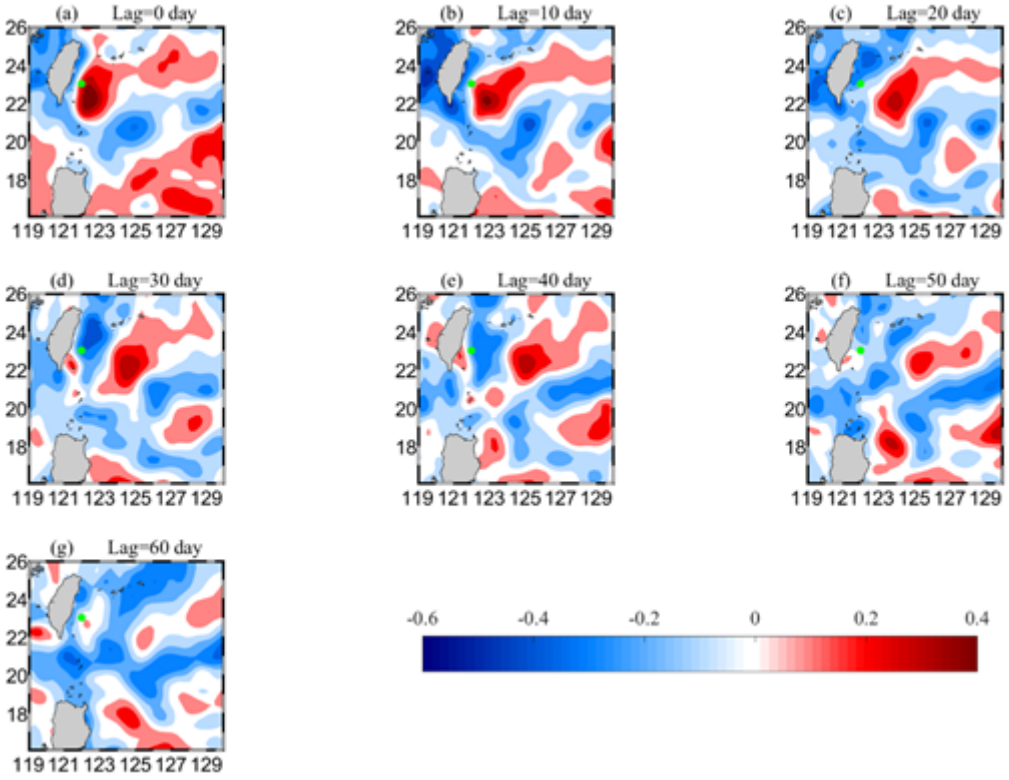

Figure 7

Maps of correlation coefficients between SLAs and minimum salinity of IW. Salinity lagged SLA by (**a**) 0 days, (**b**) 10 days, (**c**) 20 days, (**d**) 30 days, (**e**) 40 days, (**f**) 50 days and (**g**) 60 days. Color shading indicates the value of the correlation coefficient, with red (blue) indicating a positive (negative) correlation. The location of the mooring site is indicated by green dot.

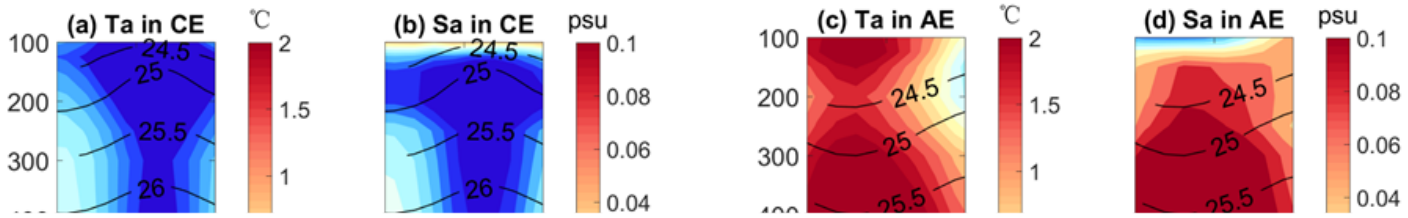

Figure 8

The structure of anticyclonic and cyclonic eddies. Temperature anomaly (**a**) and salinity anomaly (**b**) of cyclonic eddies. Colors indicate temperature and salinity anomalies, and contour lines indicate potential density (**c**) and (**d**) for anticyclonic eddies.

Figure 9

Relationship between the circulation and water mass off the eastern Taiwan. (**a**) Composite map of salinity (colors) and current (black arrows) averaged between 26.4–26.8 σ_θ east of Taiwan for cyclonic eddies and (**b**) a composite map of anticyclonic eddies. The black triangle is the mooring site.

Supplementary Files

This is a list of supplementary files associated with this preprint. Click to download.

- supplement.docx